ANNALS OF GEOPHYSICS, 67, 4, SA443, 2024; doi:10.4401/ag-9145
OPEN ACCESS

Development and Improvement of the International Reference Ionosphere with special emphasis on the topside and extension to the plasmasphere

Dieter Bilitza[*,1], Vladimir Truhlik[2], Yoshihara Omura[3], Mark B. Moldwin[4]

(1) George Mason University, Department of Physics and Astronomy, Fairfax, USA
(2) Institute of Atmospheric Physics of the Czech Academy of Sciences, Praha, Czech Republic
(3) Research Institute of Sustainable Humanosphere, Kyoto University, Kyoto, Japan
(4) University of Michigan, Ann Arbor, USA

Article history: received August 26, 2024; accepted September 19, 2024

Abstract

The International Reference Ionosphere is the international standard for Earth's ionosphere and recognized as such by the International Standardization Organization (ISO), the Committee on Space Research (COSPAR), the International Union of Radio Science (URSI) and many other organizations. This paper gives a brief introduction of the IRI model highlighting the many uses of the model in many different fields of theoretical and applied sciences and the ongoing efforts to upgrade the climatological IRI model to real-time conditions with updating indices or by assimilating data into the background IRI. The main part of the paper reviews the recent improvements and evaluations of the IRI topside electron density model and presents a new model option for extending IRI to plasmaspheric altitudes. At the heart of this new option is the use of existing empirical plasmasphere models and the Booker (1977) approach that has so successfully been applied in IRI for modelling the plasma temperatures and ion composition. Three empirical plasmasphere models are evaluated as candidates for this extension option: Carpenter and Anderson (1992), Gallagher et al. (2000), and Ozhogin et al. (2012).

Keywords: IRI; Plasmasphere; Topside; Ionosphere; Standard

1. Introduction

With more and more of our daily life depending so much on space technology it is critically important to have an accurate and reliable representation of the Earth's geo-space environment. The ionosphere is a particularly important part of geospace, because any technique that uses a probing signal travelling through these regions needs to account for the retarding and refractive effect that these regions impose on the signal. The International Reference Ionosphere (IRI) has become the internationally accepted standard for Earth's ionosphere and is recognized as such by many international organizations including the Committee on Space Research (COSPAR), the International Union of Radio Science (URSI), the International Standardization Organization (ISO) to name just

a few. The model describes the global variation of electron and ion densities and temperatures in the altitude range from about 60 km to 2000 km; the latest version (IRI-2020) also includes an extension of the electron density into the plasmasphere. Additional parameters were added in response to user requests including the vertical electron content (*vTEC*), the equatorial ion drift, the occurrence probability of spread-F, auroral boundaries, and the ratio between plasma frequency and gyro frequency. IRI is the result of several decades of international collaborations in the framework of a project jointly sponsored by COSPAR and URSI. The over 60 experts in the IRI Working Group represent different countries, different measurement techniques, and different aspects of the modelling problem. The global distribution of the membership roster shown in Fig. 1 helps to provide access to the global ionospheric data base for IRI modelling. COSPAR and URSI requested that IRI should be a data-based model, so that it would not depend on the evolving theoretical understanding of the ionospheric processes but on the accumulated data base of ground and space observations of ionospheric parameters. Over time and as new data sets became available the model was steadily improved and new versions were released at regular intervals (Rawer et al., 1978a; Bilitza, 1986, 1990, 1997, 2001; Bilitza and Reinisch, 2008; Bilitza et al., 2011, 2014, 2017, 2022). The IRI project also played an important role in recovering and analyzing older data sets (Benson and Bilitza, 2009) and in helping to resolve discrepancies between simultaneous ground and space measurements to establish the most reliable data foundation for IRI (Rawer, 1974).

IRI Working Group Members by Country

ARGENTINA: R. Ezquer, E. Gularte
AUSTRALIA: B. Ward, P. Wilkinson
BRAZIL: M. Abdu
BULGARIA: I. Kutiev
CANADA: D. Themens
CHINA: C. Xiong, J.-K. Shi, M.-L. Zhang,
CYPRUS: H. Haralambous
CZECH REPUBLIC: D. Buresova,, V. Truhlik (Chair)
FRANCE: P. Coïsson, D. Alcayde
GERMANY: W. Singer, C. Stolle, M. Hoque
INDIA: K.K. Mahajan, P.K. Bhuyan
ITALY: B. Nava, M. Pezzopane, S. Radicella, B. Zolesi
IVORY COAST: O. Obrou
JAPAN: K. Oyama, K. Igarashi, S. Watanabe
POLAND: A. Froń, A. Krankowski (URSI Vice-Chair), H. Rothkaehl, I. Stanislawska,
NIGERIA: J. Adeniyi, E. Oyeyemi
RUSSIA: A. Danilov, V. Depuev, T. Gulyaeva, A. Mikhailov, S. Pulinets, K. Ratovsky, V. Shubin, I. Zakharenkova,
SOUTH AFRICA: John Bosco Habarulema
SOUTH KOREA: Y.-S. Kwak, Y.H. Kim
SPAIN: D. Altadill. M. Hernández-Pajares
TAIWAN: J.-Y. (Tiger) Liu, S.-Y. Su, C.-K. Chao
THAILAND: P. Supniti, P. Kenpankho
TURKEY: F. Arikan
UK: M. Rycroft
UKRAINE: I. Cherniak
USA: E. Araujo-Pradere, D. Bilitza, M. Codrescu, T. Fuller-Rowell, I. Galkin (COSPAR Vice-Chair), C. Mertens, B. Reinisch, L. Scherliess, J. Sojka, S.-R. Zhang
ZAMBIA: P. Sibanda

Figure 1. List of IRI Working Group members consisting of 66 experts representing 27 countries.

When COSPAR initiated the IRI project its prime interest was in a general description of the ionosphere as part of the terrestrial environment for the evaluation of environmental effects on spacecraft and experiments in space. URSI joined the project with the goal to establish a reference model for defining the background ionosphere for radiowave propagation studies and related applications. But meanwhile IRI is used for a much wider range of applications as is documented by the large number of IRI citations (253 in 2023) in a wide range of journals covering different areas of science and engineering. Figure 2 lists the journals that have carried papers referencing IRI for their reported study. The journals are loosely grouped into several areas of specialization. Their number has increased from 62 in 2021 to 94 in 2024, clearly indicating the growing number of studies and applications across many disciplines that require a specification of the ionospheric environment and that are relying on the IRI model to provide it.

IRI, of course, is not the only model for the ionosphere and there have been quite a number of studies comparing the performance of the different models using a variety of test data and performance measures. The most extensive assessment and evaluation of different models was done by Shim et al. (2011, 2012, 2014, 2017, 2018) in the framework of the CEDAR Electrodynamics Thermosphere Ionosphere 1 (ETI) Challenge for Systematic Assessment of Ionosphere/Thermosphere Models; CEDAR is the Coupling, Energetics and Dynamics of Atmospheric Regions Program funded by the US National Science Foundation. These studies stand out because they were done by an

independent team, while many of the other ones were performed by a specific modelling team, often finding their model to be the best performing. They are also quite special because the number of models covered was larger than in most other performance comparisons and including empirical, theoretical as well as assimilative models. IRI did very well in these assessment studies. If not first than second or third in all events and cases considered using a variety of performance measures and skill scores. Recently, this effort continued with the validation study by Chou et al. (2023), who compared the measured and modelled total electron content (TEC) in the equatorial ionosphere during the 2013 March and 2021 November geomagnetic storms including empirical, physics-based, and data assimilation models (14 models in all), hosted by the NASA/NSF Community Coordinated Modeling Center (CCMC), NOAA Space Weather Prediction Center, and NASA Jet Propulsion Laboratory (JPL). They find that "GloTEC, JPL GIM, and IRI-2016 are the top three ionospheric models during the 2013 March and 2021 November storms" with an "important caveat: GloTEC and JPL GIM are not independent of the Madrigal TEC. Thus, GloTEC and JPL GIM are expected to perform better than other models." Therefore, IRI did again very well in this most recent assessment study being one of the top performers. The great success of IRI has led to several modified IRIs. Gulyaeva and Titheridge (2006) extended a modified IRI topside profile into the plasmasphere calling the model IRI-Plas. A regional update of the IRI model with data collected by a European ionosonde network, called IRI UP, was proposed by Pignalberi et al. (2018a,b). The DeepIRI (Ji et al., 2020) is based on conditional Generative Adversarial Networks trained with 48,901 GNSS TEC maps from 2001 to 2011.

IRI is a climatological model describing the spatial and temporal variations of monthly averages of the most important ionospheric parameters: electron density, ion composition (O^+, H^+, He^+, N^+, O_2^+, NO^+, Cluster ions), electron, ion and neutral temperature. Additional parameters are the ion drift at the magnetic equator, the occurrence probability of spread-F and of an F1-layer, and auroral boundaries and their dependence on magnetic activity. IRI also provides the total electron content (TEC) between user-specified upper and lower boundaries and most recently has added the ratio of plasma frequency to electron gyro frequency, an important parameter for whistler mode waves and for defining energy and frequency ranges of effective wave-particle interactions. The occurrence probability for a sporadic-E layer is the next parameter in line to be added to the IRI output.

With the increased need for accurate information about the real-time ionosphere, many studies have investigated different methods to bring IRI closer to real-time conditions. There are two main approaches: (1) Adjusting the

Traditional	Acta Geophysicae	Advances in Space Research	Advances in Radio Science
Annales Geophysicae	Geophysical Research Letters	Geomagnetism and Aeronomy	J. Geophysical Research
J. Atmos. Solar-Terr. Phys.	J. Spa. Weather & Spa. Climate	MDPI Atmosphere	Radio Science
Planetary and Space Science	Reviews of Geophysics	Solar Physics	Space Science Review
Space Weather	Surveys in Geophysics	Solar-Terrestrial Physics	Nature Communications
Earth and Planets:	Earth and Planetary Physics	Earth, Planets and Space	Global and Planetary Change
MDPI Remote Sensing	IEEE Geosci. Remote Sensing Lett.	IEEE Trans. Geosci. & Rem. Sensing	J. Asian Earth Science
IEEE Geosc. Remote Sensing Magazine	Terrestrial Atmosphere Ocean Sci	J. App. Sci. & Environ. Management	Pure & Applied Geophysi
Inter. J. App. Earth Obs. & Geoinform.	ISPRS J. Photogrammetry & Rem. Sens.	International J. Remote Sensing	Natural Hazards
GPS, GNSS, Navigation	IET Radar, Sonar, & Navigation	Journal of Institute of Navigation	GPS Solutions
Navigation	Journal of Spatial Science		
Geodesy	Geodesy and Geodynamics	J. Geospatial Inform. Technology	Journal of Geodesy
Journal of Applied Geodesy	Space Geodesy and Navigation		
Computer Science	Computer Phys. Comm.	IEEE J. Multiscale & Multiphysics Computational Techniques	
Computers & Geosciences	IEEE Access.	Astronomy and Computing	Soft Computing
Engineering Technology	Academic J . Sci. & Technology	Geosci. Instrum. Method. Data Sys.	Applied Optics
J. Machi. Manufact & Rel. Metrics	MDPI Electronics	Plasma Science & Technology	Optics Express Science
China Tech. Sci. Scientific Rep.	Proceedings of Telecom. Universities	IEEE Trans Antennas & Propagation	Technical Physics
Wireless Personal Communications	Bull. Electrical Eng & Informatics	IEICE Transactions on Communications	
Astronomy and Astrophysics	Astrophysics & Space Science	Frontiers Astronomy & Space Sci.	Cosmic Research
J. Astronomy & Space Sciences	MDPI Universe	The Astrophysical Journal	
Chemistry:	Geochimica et Cosmochimica Acta	Inter. J. Rec. Res. Phys. & Chem. Sci.	
Mathematics:	Internat. J. Numerical Modelling	MDPI Mathematics	
General Physics	International J. Physical Sciences	J. Energy Engin. Thermodynamics	Physical Review D
J. Res. & Rev. in Sci.	Physics of Plasmas	Physical Review Research	Results in Physics
J. Research and Review in Science	Progress Theo. & Exp. Physics	International J. Modern Physics B	IAIP Advances
IEEE Transactions on Nuclear Science			
National Journals:	Chinese Journal of Aeronautica	Chinese Journal of Radio Science	Chinese J. Space Science
Nigerian J. Theo. & Environ Phys	Nigerian Journal of Physics	Indian Journal of Physics	Russian J. Physical Chemistry B
Tanzania J. Science Technology	Cadernos de Astronomia	Tehnika (Serbia)	
Other:	J. Psychiatry Res. Rev. & Reports	Mon. Notices Royal Astronom. Soc.	Phil. Trans. Royal Soc. A
Discrete Dynamics in Nature & Society			

Figure 2. The long list of Journals (94 in all) that have included articles acknowledging the use of the IRI model for their reported study. They are grouped into different areas of specialization.

Reference	Indices adjusted	Parameter	Data source	Notes
Bilitza et al. (1997)	IG12	*foF2*	Global ionosonde network	Ionospheric corr. for Geosat altimeter
Komjathy et al. (1998)	IG12	*vTEC**	GPS TEC map	Altimeter ionospheric delay corrections
Hernández-Pajares et al. (2002)	IG12	*sTEC***	GPS station data	Space weather specification
Zhang et al. (2010)	Kp	Auroral boundary	GUVI/SSUSI data	Oval crossings
Pezzopane et al. (2011)	IG12	*foF2*, *M(3000)F2*	Ionosonde data	Plus assimilation of bottomside profiles
Migoya-Orué et al. (2015)	Az	*vTEC*	GIM-TEC	Interpolation between grid points
Ssessanga et al. (2015)	R12 and IG12	*vTEC*	South-Korean TEC data	Correlation between *vTEC* and *foF2*
Habarulema and Ssessanga (2016)	R12 and IG12	*vTEC*	African TEC data	Regional update for Africa
Pignalberi et al. (2018a,b)	IG12, R12	*foF2*, *M(3000)F2*	Ionosonde data	Kriging interpolation between stations
Brown et al. (2018)	Hemispheric monthly IG	*foF2*	Ionosonde network	IG-CCIR and IG-URSI
Pignalberi et al. (2024a)	IG12	*foF2* and *TEC*	Ionosonde and IONORING TEC	Regional update for Italian region
* *vTEC* = vertical total electron content; ** *sTEC* = slant total electron content along ray path.				

Table 1. Studies that have updated IRI by adjusted indices to observations.

internally used drivers (solar, ionospheric, or magnetic indices) so that the IRI F2-peak or IRI TEC values agree with measured values. (2) Using a mathematical technique (Kalman Filter, variational methods) for assimilating measurements into the background IRI model. Tables 1 and 2 list some of the studies applying the adjustment and assimilation techniques, respectively. A comprehensive review of the adjusting approach (1) was given by Pignalberi et al. (2018a, b).

In the following sections this paper discusses the recent improvements and assessments of the IRI topside electron density profile and presents an extension of the IRI profile to plasmaspheric heights with the help of available empirical plasmasphere models. A reliable description of these two regions is critically important for the many space technology applications that use radio waves travelling through all or part of the ionosphere-plasmasphere environment.

2. Improvements of the IRI Topside Electron Density Profile

The topside ionosphere is the region from the point of highest density, *NmF2*, to the top of the ionosphere at about 2000 km. An accurate representation of the electron density in this region is of particular importance because it contains the largest densities and therefore causes the largest effects on the transversing waves that so many space technologies are using. But density measurements in this region are much fewer than below *NmF2*, because the ever-increasing network of ground-based ionosondes can only measure up to *NmF2*. The incoherent scatter

Reference	Parameter(s) assimilated	Data source	Method	Notes
Fridman et al. (2006)	*TEC*	GPS data	Tikhonov method	GPSII model
Schmidt et al. (2008)	*TEC*	GNSS, TOPEX/Jason	Multi-dimensional B-spline	Also Zeilhofer et al. (2009)
Angling et al. (2009)	*TEC*	GPS data	Minimum variance technique	EDAM model
Galkin et al. (2012 and 2020)	*foF2*, *hmF2*	GIRO ionosondes	NECTAR morphing algorithm	IRI Real-Time Ass. Mapping (IRTAM)
Yue et al. (2012)	*TEC*, *foF2*, *hmF2*	GNSS, Jason 1, 2, ROD* from CHAMP, GRACE, COSMIC, SAC-C, Metop-A, TerraSAR-X	Kalman filter technique	Reanalysis for 2002-2011
Wenjing et al. (2015)	*NmF2*, *hmF2*	GNSS data	4-d variance estimation method	Regional modelling
Aa et al. (2016)	*TEC*	GNSS, COSMIC ROD	3-d variational technique	Regional model for China
Lin et al. (2017)	*TEC*	GPS, COSMIC ROD	Gauss-Markov Kalman filter	COSMIC 2 improvement
Ssessanga et al. (2019)	*TEC*	South African TrigNet	4-d var technique	Imaging region ionosphere
An et al. (2019)	*vTEC*	Jason-2/-3, GNSS	Spherical harmonic expansion	> 300 GNSS stations
Mengist et al. (2019)	*sTEC*, *NmF2*	GNSS, COSMIC ROD, ionosondes	Ionospheric Data Ass. 4-D (IDA4D)	Period analyzed 15-18 March 2015
Jeong et al. (2022)	*sTEC*, *NmF2*	GPS, COSMIC	Ionospheric Data Ass. 4-D (IDA4D)	Regional model South Korea
Lv et al. (2022)	*vTEC*	GNSS	Kalman filter	For better HF applications
Hu et al. (2024)	*NmF2*, *hmF2*, *B0*, *B1*, *vTEC*	COSMIC 1, 2 ROD, NGDC ionosondes, Jason 2, 3	Spherical harmonic expansion for obs. hmF2, B0, B1	Optimal IG12 to to fit global vTEC data
Mao et al. (2024)	*TEC*	ALOS-1 SAR images	Integrating Time Series InSAR (TS-InSAR) with IRI	Novel TEC mapping method
* ROD = Radio Occultation Data.				

Table 2. Studies discussing assimilative techniques with various data source and IRI as background model.

radars are able to measure topside electron densities but only a very small number of such radars exists due to the high coasts and energy needs. With the advent of satellites, it became possible to carry the ionosonde above the F2 peak and measure densities from the satellite down to *NmF2*. The Aloutte 1,2 and ISIS 1,2 satellites were able to gather information about the topside with these ionosonde-like instruments, called topside sounders, for more than two solar cycles from the 1960s to the 1980s. In fact, the data base collected by far outpaced the data analysis capabilities at the time. Only recently with modern technology and with strong encouragement from the IRI team was the analysis effort taken up again and resulted in almost doubling the previously existing volume of topside electron density profiles (Bilitza et al., 2004; Benson and Bilitza, 2009). Numerous satellites have made in situ observations of the electron density in the topside ionosphere. However, in situ measurements provide the

absolute electron density while for the IRI topside profile the relative density normalized to the F2 peak density and height is needed. Therefore, an IRI misrepresentation of the in-situ observations can be due to the NmF2, hmF2, or topside model (Bilitza et al., 2012).

Because of the importance of the topside region for *TEC*, empirical topside modelling has been a very active field, a lot of it focused on the representation of the topside scale height (e.g., Stankov and Jakowski, 2006; Liu et al., 2008; Li et al., 2019). Some of the more recent models include the model of Prol et al. (2018) based on GPS radio occultation data, of Prol et al. (2019) using the Vary-Chap formalism of Reinisch et al. (2007) with topside sounder and radio occultation data and the Neural network-based model of Smirnov et al. (2023) trained with 19 years of GNSS radio occultation data. Several studies have proposed NeQuick-based topside models that will be discussed in the NeQuick paragraph below.

IRI offers four options for the topside profile, they are called IRI2001, IRI2001cor, NeQuick, and COR2. The IRI2001 option goes back to the early work of Rawer et al. (1978a, 1978b, 1978c) and Rawer (1984), who used Epstein functions for an analytical representation of the Bent et al. (1972) model. They were, however, working with a quite limited data base consisting only of about 40,000 Alouette-1 topside sounder profiles resulting in an overestimation of electron density in the upper topside by the IRI model and leading to unrealistically steep topside profiles especially at higher latitudes and high solar activities. Noting the limited amount of available topside profiles the IRI team strongly supported a data restoration project of Alouette 1,2 and ISIS 1,2 topside sounder data (Bilitza et al., 2004; Benson and Bilitza, 2009). With the large volume of topside sounder data that became available Bilitza (2004) was able to determine a correction factor for the IRI2001 topside model that lowered the IRI electron densities in the upper topside and thus resulted in more realistic profiles. The new option was called IRI2001cor.

The NeQuick model evolved out of a series of models developed by Radicella and Leitinger (2001) using theoretical considerations and relationships between profile and peak parameters established with ionosonde data. The topside part is represented by an Epstein layer function with varying scale height and a base scale height that is related to the bottomside scale height. With the help of the newly available ISIS topside sounder data the NeQuick topside model was upgraded to Version 2 (Coïsson et al., 2006; Nava et al., 2008) and was introduced as the NeQuick topside option into IRI (Bilitza and Reinisch, 2008). A number of studies have proposed further improvements of the NeQuick topside model. Themens et al. (2018) determined NeQuick parameters for middle and high Northern latitudes based on incoherent scatter radar data, Gravity Recovery and Climate Experiment (GRACE) and COSMIC radio occultation data, and the Alouette/ISIS topside sounder data. Pezzopane and Pignalberi (2019) used Swarm in situ measurements to obtain a new formulation for the NeQuick base scale height parameter H_0. Pezzopane et al. (2024) continued this work developing a new analytic representation of H_0 based on Swarm data and updated IRI maps for *foF2* and *hmF2*. Singh et al. (2021) and Pignalberi et al. (2022) deduced NeQuick topside parameters from COSMIC radio occultation data, which could serve as input for future improvements of the NeQuick option.

Bilitza (2009) evaluated the three topside options IRI2001, IRI2001cor, NeQuick with the full Alouette/ISIS topside sounder data base of over 160,000 profiles. He found that overall, the NeQuick option gives the best results and it was implemented as the recommended IRI default option. However, he also found that IRI2001cor provides a more realistic representation of the altitudinal-latitudinal structure in the equatorial ionization anomaly (EIA) region. With IRI2001cor the EIA latitudinal structure near the F2 peak with crests on both sides of the magnetic equator correctly merges into a single peak at the magnetic equator at high altitudes, while in the case of NeQuick the dependence of profile parameters on F2 peak parameters propagates the double-peak structure to higher altitudes. Pezzopane at al. (2023) discussed potential solutions to the NeQuick mismodeling problem of the upper EIA region.

A major new improvement cycle for the IRI topside model started when Lühr and Xiong (2010) reported that all three options significantly overestimated Challenging Minisatellite Payload (CHAMP) satellite and GRACE satellite in situ measurements during the 2008-2009 solar minimum period of cycle 23. Similar results were then also reported by Klenzing et al. (2011, 2013) and Bilitza et al. (2012) comparing IRI predictions to in situ data from the Communication/Navigation Outage Forecast System (C/NOFS) satellite. And further confirmation came from the study of Migoya-Orue et al. (2013) with data acquired by the Special Sensor-Ions, Electrons, and Scintillation (SSIES) package aboard the Defense Meteorological Satellite Program (DMSP) spacecrafts F13 and F15. The Cycle 23 minimum was exceptional in that it reached lower values than previous minima and in that it ended in an extended minimum period that proved all predictions wrong. IRI was developed with data from previous cycles and thus lacked the ability to represent electron densities during this exceptional solar minimum. The topside profile is normalized to the F2 peak density *NmF2* and height *hmF2* and thus the misrepresentation could be caused by either

one or all of three models: the *NmF2* model, the *hmF2* model and/or the topside profile model. Bilitza et al. (2012) presented good evidence that the topside profile model is the major culprit with some minor impact by the *hmF2* model. Using the Alouette/ISIS topside sounder data base together with the data base of in situ measurements from CHAMP, GRACE, and Swarm, Bilitza and Xiong (2021) were able to determine a solar-activity dependent correction term for the IRI2001cor option that overcame the problem at low solar activities. With this new option, called COR2 or IRI2001cor2, good agreement was achieved with the very low electron densities reached during the 2008-2009 solar minimum.

An extensive validation study of the four IRI topside options was undertaken by Pignalberi et al. (2024b) involving comparisons with in situ observations by GRACE, by the Ionospheric Connection Explorer (ICON) and by the DMSP F15 satellite. Their combined data base spans the time period 1999 to 2022, covering different diurnal, seasonal, and solar activity conditions, on a global basis in the altitude range 400-850 km. They find that NeQuick and COR2 show the best performance, with COR2 marginally better at the ICON and GRACE altitudes, 400-600 km, while NeQuick performs slightly better at the DMSP altitude of 830-850 km. There is room and need for further improvement as pointed out in this study. The COR2 option, while describing the low latitude topside with associated EIA phenomenology remarkably well, still shows a solar activity trend in the upper topside. The NeQuick option represents the lower and upper topside quite well, but still needs to counter-balance the propagation of the EIA features to higher altitude.

3. Extension of the IRI Electron Density Profile into the Plasmasphere

One of the most important ionospheric parameters for many space technologies is the total electron content (TEC) encountered by the probing radio wave travelling from satellite to ground or vice versa, because the electron gas delays and refracts the propagating radio wave. For the ever more important Global Positioning Satellite (GPS) systems the impact of TEC (between satellite transmitter and ground receiver) is the largest error source. If the satellite is orbiting in the plasmasphere or above then in addition to the ionospheric part of *TEC* (*ITEC*) the contribution of the plasmaspheric plasma to *TEC* (*PTEC*) has to be considered. GPS satellites, for example, fly at an altitude of approximately 20,200 km way above the plasmasphere and therefore a good knowledge of the ionospheric and plasmaspheric electron densities is essential. For the ionospheric part IRI is the accepted international standard and *ITEC* can be obtained by calculating and then integrating the IRI electron density values along the ray path from satellite to the ground.

Different methods have been used to add PTEC to the IRI-computed ITEC. Early studies just ignored the PTEC contribution arguing that it is negligibly small compared to ITEC. At nighttime, however, the *PTEC* percentage of TEC can reach 40-50% and even during daytime neglecting the small plasmaspheric contribution will lead to reduced *TEC* accuracy. Other studies, noting that *PTEC* does not show a significant diurnal variation, used a constant *PTEC* value for satellites orbiting above the plasmasphere and assumed an exponentially decreasing profile with a constant scale height for satellites orbiting at plasmaspheric altitudes (e.g., Bilitza et al., 1988). Extrapolating the ionospheric topside profile into the plasmasphere was another popular method and best results were achieved with the NeQuick topside formula which is also an option for IRI model users. Gulyaeva (2003) proposed an alternate IRI topside electron density profile by introducing an anchor point at the topside half-width, the height where $N_e = 0.5 \cdot NmF2$, and used Chebyshev functions to describe its variation with geomagnetic latitude, local time and solar activity. The extension into the plasmasphere of this modified IRI model was introduced by Gulyaeva and Titheridge (2006) and was given the name IRI-Plas. All of these methods, however, are strongly tight to the topside electron density profile formalism with little input and usage of measurements of the electron density at plasmaspheric heights.

Noting the importance of including observed densities the IRI team from early on encouraged the intercomparison of different measurement techniques as a first step (e.g., Williams et al. 1981). Rycroft and Jones (1985, 1987), in their studies, set out to develop a plasmasphere model specifically for IRI. Their Diffusive Equilibrium (DE) Model described the electron density along geomagnetic field lines based on the electron temperature model that Strangeway (1986) had developed with satellite observations and incoherent scatter radar data. Kimura et al. (1996) used a similar approach but modified the Strangeway (1986) model to obtain agreement with his Akebono wave data. Since than a number of empirical plasmasphere models have been developed using different modelling technique and different data sources. A good recent review and comparison of the different models was given by Ripoll et al. (2023). In the next subsection we will discuss three of the most frequently used empirical plasmasphere

models as potential candidates for the extension of IRI in the plasmasphere. Section 3.2 introduces our data sources for evaluating these models, Section 3.3 presents the results of our evaluation and Section 3.4 explains the approach for connecting these models to the IRI topside electron density profile.

3.1 Empirical Plasmasphere Models Evaluated in this Study

Over the last decades a number of empirical plasmaspheric models have been developed based on different data sources and different theoretical assumptions. Denton et al. (2006) used a power law form to describe the field line plasma distribution with Polar and CRRES data. The model developed by Jakowski and Hoque (2018) with electron density data deduced from CHAMP-GPS measurement consists of an upper L-dependent part and a lower altitude-dependent part and both using an exponential decay. Zhelavskaya et al. (2017) trained a Neural Network with the database that they had obtained from the Electric and Magnetic Field Instrument Suite and Integrated Science (EMFISIS) instrumentation on the Van Allen Probe satellite with the Neural-Network-based Upper hybrid Resonance Determination (NURD) technique. Prol et al. (2022) used an Epstein transition function with varying scale height to represent the NURD density data. Combining Van Allen Probes data for latitudes below 20° with Arase data up to 40° for $1 < \mathrm{L} \leq 3$, Hartley et al. (2023) developed a new electron density model with both latitudinal and Magnetic Local Time (MLT) dependence.

A modular approach is common to most models combining sub-models for the different distinct plasmasphere regions: from the inner plasmasphere to the steep gradient at the plasmapause, and the much lower densities in the trough region. An assessment and evaluation of these models with a set of reliable data sources is the first step towards implementation of one of these models into IRI.

As noted earlier the current options proposed for a plasmaspheric extension of IRI are either based on an extrapolation of the topside formula or are normalized to an electron density and temperature foot-point in the topside. It is, however, important that both regions are modelled independently with the data base available for each region and in a second step the models can then be merged with appropriate mathematical functions. We have selected three models partly because they are three of the most frequently cited plasmasphere models and partly because they rely on different data sources and thus give some indication of still existing uncertainties. The three are the models developed by Carpenter and Anderson (1992), Gallagher et al. (2000), and Ozhogin et al. (2012) and thus they also document the progress made in plasmaspheric modelling over these years.

The model developed by Carpenter and Anderson (1992), from now on called CA1992, is one of the first and most widely used empirical model for the whole plasmasphere. It combines in piecewise fashion models for the inner plasmasphere, the region of steep plasmapause gradients, and the plasma trough. Their model for the inner plasmasphere describes the exponential decrease of the equatorial electron density N_e with increasing L-value and includes second order terms depending on season (D = day of year) and solar activity (S = F10.7) and the falloff of these terms with increasing L

$$\log_{10} N_e(L, D, S) = (-0.3145\, L + 3.9043) + \left[0.15 \left(\cos\left\{\frac{2\pi(\mathrm{D}+9)}{365}\right\} - 0.5\cos\left\{\frac{4\pi(\mathrm{D}+9)}{365}\right\}\right) + 0.00127\,\mathrm{S} - 0.0635\right] \exp\left\{-\frac{L-2}{1.5}\right\}. \quad (1)$$

The model is based on electron density profiles deduced from sweep frequency receiver (SFR) radio measurements by the International Sun-Earth Explorer (ISEE) satellite and on previously published results from Whistler measurements. Variations with local time are not considered in the model, which is an acceptable assumption above $L = 2$ due to the large fluxtube electron content that will not be affected much by upward flux from the ionosphere.

Gallagher et al. (2000) also use a modular approach with their Global Core Plasma Model (GCPM) combining separately developed models for the plasmasphere, plasmapause, trough, and polar cap regions. In addition, they connect their model to IRI using exponential extrapolations from both sides and a hyperbolic tangent merging function. GCPM describes the plasma density, temperature and composition as a function of L-value, season, and magnetic and solar activity indices and relies predominantly on data from the Retarding Ion Mass Spectrometer (RIMS) and Plasma Wave Instrument (PWI) that flew on the Dynamics Explorer 1 (DE 1) satellite. They use the

formular of Carpenter and Anderson (1992) for the inner plasmasphere (Equation (1)) with coefficients for the main L-dependence fitted to their data base. The model, from here on called GA2000, is given by the formula:

$$\log_{10} N_e(L, D, S) = (-0.79\, L + 5.3) + \left[0.15\left(\cos\left\{\frac{2\pi(\mathrm{D}+9)}{365}\right\} - 0.5\cos\left\{\frac{4\pi(\mathrm{D}+9)}{365}\right\}\right) + 0.00127\,\mathrm{S} - 0.0635\right]\exp\left\{-\frac{L-2}{1.5}\right\}. \quad (2)$$

Ozhogin et al. (2012) developed their model, from here on named OZ2012, based on density data derived from active sounding along magnetic field lines by the Radio Plasma Imager (RPI) on the Imager for Magnetopause-to-Aurora Global Exploration (IMAGE) satellite from June 2000 to July 2005. With the field-aligned RPI data it was for the first time possible to fully study the electron density distribution along magnetic field lines. Reinisch et al. (2004) found that the field-aligned density distribution can be treated neither as constant nor as a simple diffusive equilibrium distribution profile as in many of the earlier models including the CA1992 and GA2000 models. Instead, good agreement was obtained with a functional form that describes variation with the invariant latitude of the magnetic field line λ_{INV}, which is related to L by $\lambda_{INV} = \mathrm{arc\ cos}\ \{\mathrm{sqrt}(1/L)\}$ and the magnetic latitude λ along the field line:

$$\log_{10} N_e(L, \lambda) = (-0.4903\, L + 4.4693) + \log_{10}\left[\cos^{-0.75}\left\{\frac{\pi}{2}\frac{(1.01\,\lambda)}{\lambda_{INV}}\right\}\right]. \quad (3)$$

Ozhogin et al. (2012) used their data base also to study variations with MLT and found as expected that the MLT dependence becomes more pronounced for field lines closer to the ionosphere. But even for L shell values less than 2.5 the difference between noon and midnight densities is below the data fluctuation level. They also did not observe significant dependence on geomagnetic and solar activity indices. But that may be possibly due to the insufficient data coverage at high levels of geomagnetic activity and of a full solar cycle.

It is important to note that the OZ2012 model is the only one of the three models that describes density variations along a magnetic field line. The other two models assume a constant electron density along a magnetic field-line. This makes OZ2012 quite unique compared to many of the existing plasmasphere models, as Ripoll et al. (2023) pointed out in their review.

3.2 Data Used to Evaluate the Plasmasphere Models

The plasmasphere like the topside ionosphere is a region where there is a urgent need for more data to cover the large volume in space that is taken up by this part of our planet's plasma environment. Three data sets were used for this study. The main criteria for selecting these data sets were: (1) Data acquired with different techniques; (2) Data from different satellite missions and if possible different solar cycle periods; (3) Data that had been used in a number of studies and publications. Based on these criteria for our assessment study we have utilized data acquired by the Dynamics Explorer 1 (DE-1) satellite, the Combined Release Radiation Effects Satellite (CRRES), and the Imager of Magnetopause-to-Aurora Global Exploration (IMAGE). They will be introduced in more deatil in the next paragraphs.

DE-1 was launched on August 3, 1981, orbited earth in a highly elliptical orbit with an apogee of 23,289 km, a perigee of 567 km and an inclination of 89.9°, and was deactivated on February 9, 1991. The DE-1 data used here are from the Retarding Ion Mass Spectrometer (RIMS) instrument for the time period from October 8, 1981 to December 30, 1984 including 36,302 data points. The data set is available from NASA's Space Physics Data Facility (SPDF) at https://spdf.gsfc.nasa.gov/pub/data/de/de1/plasma_rims/. It includes the densities and temperatures of O^+, H^+, He^+, O^{++} and He^{++} ions and assuming charge neutrality we get the electron density by summing over all ion densities.

CRRES was launched on July 25, 1990 into a geosynchronous transfer orbit with a perigee of 347 km, an apogee of 33,293 km, and an inclination of 18.15°. Contact was lost to the spacecraft on October 12, 1991. Electron density data were obtained by the onboard Plasma Wave Experiment of Anderson et al. (1992). For our assesment we used CRRES electron density data from the time period August 19, 1990 to October 12, 1991 comprising of 2,645,855

data points. The data set was provided by M. Moldwin and can be accessed at the University of Michigan Deep Blue Data repository (Moldwin, 2024).

The IMAGE satellite was launched on March 25, 2000 into a polar orbit with a perigee of 1000km and an apogee of 46,004 km and unexpectedly ceased operation in December 2005. Our third data set are the electron density data obtained by the Radio Plasma Imager (RPI) onboard the IMAGE satellite. But these are not the field-aligned data that were used for developing the Ozhogin et al. (2012) model. For the assessment we make use of the passive electron density measurements that were determined in situ from the RPI dynamic spectra. The data set covering the time period from January 1, 2001 to December 18, 2005 and consisting of 204,786 data points was obtained from SPDF (https://spdf.gsfc.nasa.gov/pub/data/image/rpi/rpi_Ne_fp_along_orbit/). A detailed description of how the data were determined is given by Webb et al. (2010).

3.3 Model Assessment

For assessing the performance of the three plasmasphere models with the three data sets, we first need to determine the subset of each data set that is within the plasmasphere. All three satellites were highly elliptical and therefore spend only parts of their orbits in the plasmasphere. For the lower boundary we selected 2000 km, which is the top of the core IRI model. The outer boundary of the plasmasphere is the plasmapause, where the electron density drops dramatically by at least half an order of magnitude. We use the data acquired up to this boundary for our assessment. Quite a number of models have been developed for the location of the plasmapause, mostly depending on MLT and L and based on data from a specific satellite instrument. Comparisons and reviews of the different models can be found in Pierrard et al. (2021) and Guo et al. (2021). One of the earliest and often used model for the location of the plasmapause is the one introduced by Carpenter and Anderson (1992) as part of their plasmasphere model

$$L_{pp} = 5.6 - 0.46\, Kp_{max24} \tag{4}$$

Here L_{pp} is the L-value of the plasmapause field-line and Kp_{max24} is the maximum Kp index observed during the previous 24 hours. For this study the plasmapause model of Moldwin et al. (2002) was used that is based on one of the data sets used for our model assessment, the CRRES/PWR data. With this large data base, they were able to fit formula (4) to the data in different time zones obtaining

$$L_{pp} = 5.70 - 0.420\, Kp_{max12} \quad \text{for LT} = 21{:}00\text{-}03{:}00 \quad \text{midnight} \tag{5a}$$

$$L_{pp} = 6.05 - 0.573\, Kp_{max12} \quad \text{for LT} = 03{:}00\text{-}09{:}00 \quad \text{dawn} \tag{5b}$$

$$L_{pp} = 5.20 - 0.425\, Kp_{max12} \quad \text{for LT} = 09{:}00\text{-}15{:}00 \quad \text{noon} \tag{5c}$$

$$L_{pp} = 4.45 - 0.167\, Kp_{max12} \quad \text{for LT} = 15{:}00\text{-}21{:}00 \quad \text{dusk} \tag{5d}$$

The model describes the most persistent variation patterns of the plasmapause including the increase with decreasing magnetic activity and the dusk sector bulge that rotates towards noon with increasing geomagnetic activity. There is significant variability in the location of the plasmapause. The average standard deviation noted by Moldwin et al. (2002) is $L_{SD} \approx 0.7$ and the correlation is as low as 0.26 for the dusk period and the highest (0.7) for dawn and noon. These uncertainties will only have a minor effect on the data selection for the model assessment, but they will make it difficult to construct an IRI electron density profile with the steep plasmapause drop at the correct location.

With the data sets limited to the plasmasphere region we have produced plots that show the distribution of the percentage difference between data and models. In Fig. 3 the distributions for all three plasmasphere models are displayed for the CRRES PWE data set, which consisted of 533,988 data points within the plasmasphere. The x-axis is divided into 10% bins and the y-axis shows how many data-model errors were sampled in each bin. For example, if we look at the 0-10% error bin in Fig. 3, the CA1992 model is representing about 40,000 data points with this percentage accuracy, the OZ2012 for about 38,000 data points, and the GA2000 only for about 22,000 data points. Also listed are the medians and standard deviations and the percentage bins where each distribution peaks. CA1992 is the best performer slightly better than the OZ2012 model, while the GA2000 model lags behind the other two. The same order is also documented by the medians, the standard deviations, and the percentage maxima. The medians and distributions indicate that GA2000 clearly underestimates the CRRES data while CA 1992 and OZ2012 slightly overestimate the data.

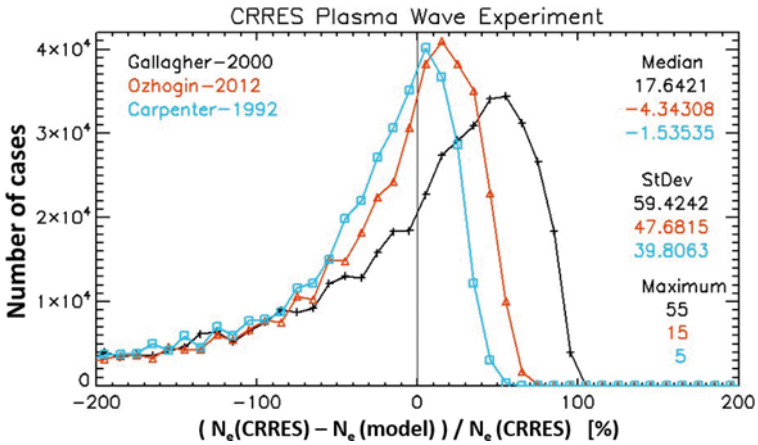

Figure 3. Percentage error distribution between the CRRES PWE data and the three models: Gallagher et al. (2000), Ozhogin et al. (2012), and Carpenter and Anderson (1992). A point (x,y) on the curves indicates the number of cases (y) with a percentage error of x ± 5%. Also listed are the medians, standard deviations and peak percentages for all three models. The total number of data points within the plasmasphere is 533,988.

Figure 4 presents the percentage error distributions for the IMAGE RPI data consisting of 56,129 plasmaspheric data points. The OZ2012 shows the best performance as documented by the distribution as well as the medians and peak percentages. This, of course, could be expected, because RPI data were used for the OZ2012 model development. But one has to keep in mind that these are two different RPI data sets. Ozhogin et al. (2012) used the data obtained from soundings along field lines for their model development, while the assessment data are obtained from the in-situ measurements along the spacecraft orbit. OZ2012 slightly overestimates the data, while the other two underestimate the RPI data with the GA2000 median lower than the CA1992 median.

The assessment distributions with the DE-1 RIMS data are shown in Fig. 5. The limitation to below the plasmapause reduced the number of data points to 24,119, an order of magnitude smaller than the data volume available from CRRES/PWE and a factor of two smaller compared to the IMAGE/RPI plasmasphere data set. For CA1992 and OZ2012 the error distributions show a peak structure somewhat similar to the ones seen in Figs. 4 and 5. For GA2000 the distribution is relatively flat with a small peak at –5%. The standard deviations for all three models are large than for the other two data sets indicating that all three models have problems representing this data set. This is a somewhat surprising result for the GA2000 model, because the DE-1/RIMS data were an important part of the data foundation for this model. The disagreement of GA2000 with the RIMS data may be due to the fact that we only use the main plasmasphere part of the GCPM and not the other parts. At lower altitudes the connection region to the IRI topside profile will lead to difference between the GCPM prediction and the GA2000 model that we are using and could possibly lead to better agreement with the RIMS data. And the same is true for the upper part where the GCPM internally models the plasmapause region, which could lead to differences between the GCPM values and our GA2000 values and thus also affect the data-model comparison outcome. All three distribution show a much slower drop-off at negative percentages than for the other two data sets which also points to the difficulty all three models have with this data set.

A common feature that can be seen for all three models with all three data sets is the asymmetry of the distribution of percentage residuals, with a much longer tail in the negative part of the distribution. This indicates a systematic overestimation of all three data sources by all three models and is also documented by the mostly negative median values. This could be due to shortcomings of the models or to problems of the data sets. Since the three data sets were obtained with different measurement techniques on different satellites an error source common to all three seems unlikely. The three models, on the other hand, are all using the mathematical formalism introduced by Carpenter and Anderson (1992) for describing the dependence on *L*. They assume a linear relationship between the decadic logarithm of the electron density and the *L* value (Formula (1)). This is a relatively good approximation for the average across many profiles as the corresponding figures in all three model papers show. The two other models use the same relationship but obtain different regression parameters when fitting the formula to their data sets (Formulas (2), (3)). The need for different parameters could be due to spatial or temporal biases of the satellite data set that was used for developing a specific model. It could also indicate that the Carpenter-Anderson formula misses additional dependencies that could explain the variation in the regression parameters between the different models.

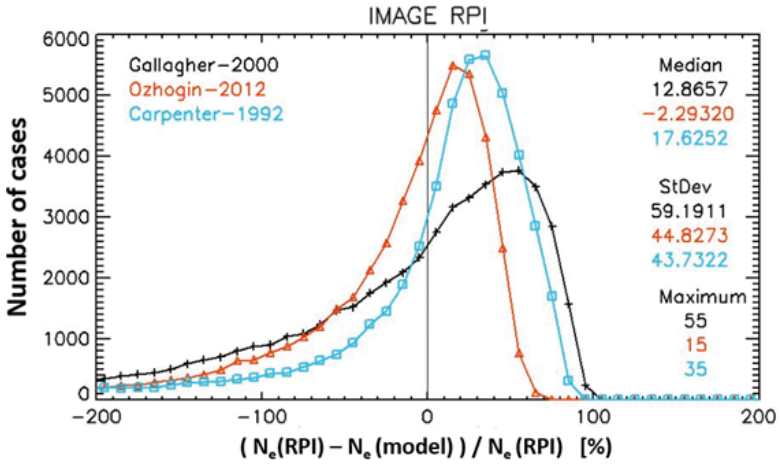

Figure 4. Percentage error distribution between the IMAGE/RPI data and the three models: Gallagher et al. (2000), Ozhogin et al. (2012) and Carpenter and Anderson (1992). A point (x,y) on the curves indicates the number of cases (y) with a percentage error of x ± 5%. Also listed are the medians, standard deviations and peak percentages for all three models. The total number of data points within the plasmasphere is 56,129.

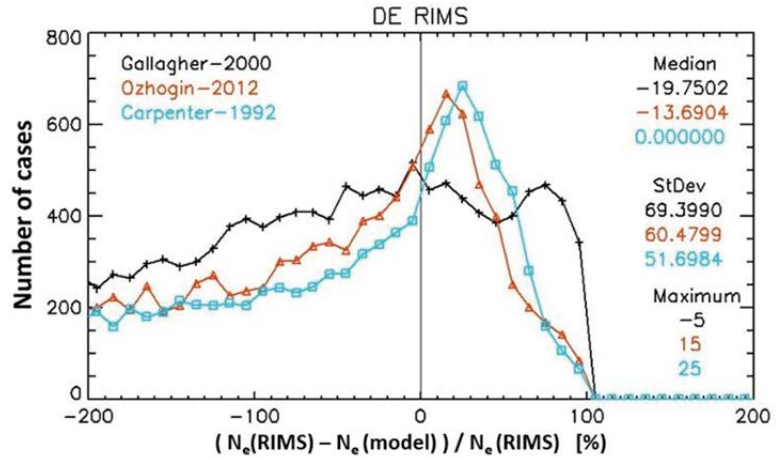

Figure 5. Percentage error distribution between the DE-1 RIMS data and the three models: Gallagher et al. (2000), Ozhogin et al. (2012) and Carpenter and Anderson (1992). A point (x,y) on the curves indicates the number of cases (y) with a percentage error of x ± 5%. Also listed are the medians, standard deviations and peak percentages for all three models. The total number of data points within the plasmasphere is 24,119.

Ignoring the somewhat unusual results obtained with the RIMS data, we find that the OZ2012 model shows the best results with the CA1992 model a close second. As Ripoll et al. (2023) pointed out OZ2012 is also the only model that explicitly includes latitudinal dependence. Therefore, we recommend using the OZ2012 model as the default for the extension of the IRI model into the plasmasphere and the other two models can be introduced as additional options. For the development and subsequent improvement of IRI the use of model options for specific regions has been very successfully applied. With the help of user-specified switches the default model for a specific region can be replaced by one or two other models. In this way users can participate in the evaluation of the different models with their specific data set.

3.4 Approach for Extenting IRI into the Plasmasphere

The approach for connecting the plasmasphere models to the standard IRI model makes use of Epstein transition functions in similar fashion as is done for the plasma temperatures and ion composition in IRI (Truhlik et al., 2012, 2015, 2021). This unique approach was first proposed by Booker (1977) for his study of radio wave scattering in the ionosphere. The approach divides a profile into sections of almost constant gradient getting the so-called 'skeleton profile'. Then Epstein step functions are used to connect the different sections, getting an analytical representation of the skeleton profile. Integrating this analytical function for, in our case, the electron density gradients one than gets an analytical representation of the whole electron density profile. For a profile with N sections of constant gradients g_i the Booker function B becomes

$$B(h; h_0, g_i, HX_i, SC_i) = B_0 + (h - h_0)g_1 + \sum_{i=1}^{N} (g_{i+1} - g_i)\, SC_i [EPS\_1(h; HX_i, SC_i) - EPS\_1(h_0; HX_i, SC_i)] \quad (6a)$$

$$EPS\_1 = \ln\left\{1 + \exp\left[\frac{(h - HX_i)}{SC_i}\right]\right\} \quad (6b)$$

with the section boundaries HX_i and the transition thicknesses SC_i, and the integration taken from h_0 (which is the base point of the profile) to h. A detailed description of the approach can be found in Appendix A of Bilitza et al. (2022).

The Booker (1977) approach has been successfully applied for modelling the IRI plasma temperatures and the IRI ion composition. And indeed, it was also used for the development of the topside options IRI2001cor and COR2. In IRI2001cor the altitudinal variation of the correction term is describes with the Booker approach. The COR2 option makes use of Booker's method to describe the variation of its solar activity linear regression parameters with modified dip latitude and altitude. We propose to extend the IRI2001cor approach from the topside into the plasmasphere with additional fixpoints (called also anchor points) in the plasmasphere and to use one of the evaluated plasmaspheric models to obtain the electron density at these fixpoints. The plasmapause location would be an obvious choice for one of these fixpoints. However, the actual location can vary significantly from the average location given by the plasmapause models as discussed in section 3.3. There are also still some differences between the numerous mostly satellite-mission-specific plasmapause models. We tested different sets of plasmaspheric fixpoints with and without the plasmapause location using the OZ2012 model to determine the electron density at the fixpoints and using comparisons with the IMAGE/RPI data as evaluation criteria. Very good results were achieved with fixpoints at 5,000 km, 10,000 km, 20,000 km and 30,000 km. Because of the connection to the IRI2001cor option our proposed plasmaspheric extension approach can only be used with the IRI2001cor and the COR2 topside options, and is not applicable for the IRI2001 and NeQuick options. For the NeQuick option the plasmaspheric extension is achieved by extrapolation of the topside profile into the plasmasphere.

In Fig. 6 the resulting error distribution with the set of the above indicated fixpoints and the OZ2012 model is compared to the error distribution obtained with the extrapolation of the NeQuick topside option. The fixpoint version exhibits a broader distribution but provides a significantly better agreement with the IMAGE/RPI data than the NeQuick extrapolation. The NeQuick underestimation at plasmaspheric heights shown in Fig. 6 confirms earlier results by several other authors. Kashcheyev and Nava (2019) studied the NeQuick behavior in the topside ionosphere – plasmasphere region by comparing *vTEC* in the altitude range 800 km to 20,000 km with corresponding COSMIC-1 data obtained using the precise orbit determination antennas. They found that NeQuick underestimates

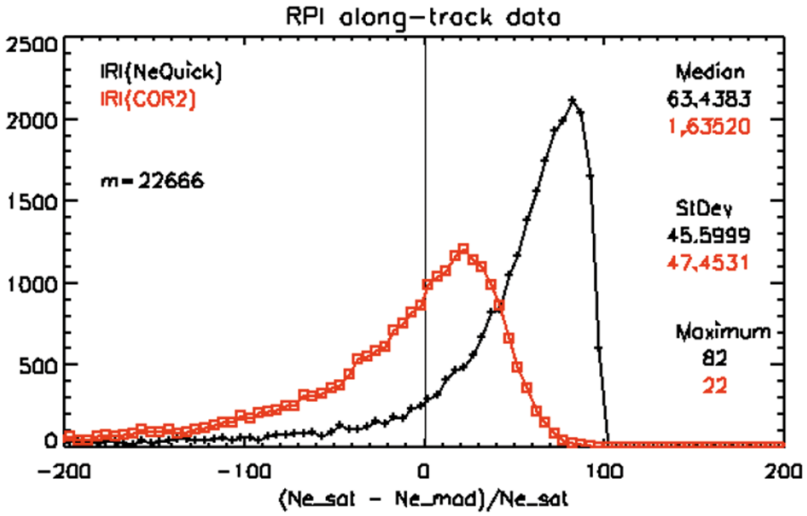

Figure 6. Percentage error distribution between the IMAGE/RPI data and the IRI model using the COR2 option for the topside and the plasmaspheric extension proposed in this paper (red squares) and the IRI model using the NeQuick topside option and extrapolating it to plasmaspheric heights (black crosses). A point (x,y) on the curves indicates the number of cases (y) with a percentage error of x ± 2.5%. Also listed are the medians, standard deviations and peak percentages for both cases. The total number of data points considered is m = 22,666.

the COSMIC-1 data by 2 to 8 TECU (average 3.73 TECU). A similar result was obtained by Pezzopane and Pignalberi (2019), who compared NeQuick predictions with *vTEC* obtained by the Swarm B satellite and found underestimations by NeQuick in the range of 3 to 6 TECU depending on solar activity conditions. Results that were further confirmed by a follow-on study by Pezzopane et al. (2024). More recently Servan-Schreiber et al. (2024) reported similar results by comparing the model with TEC measured by several GNSS ground receiver stations at different latitudes. This study highlighted also the improvement achieved with the inclusion of plasmaspheric models in IRI.

It should, however, be noted that our approach includes several approximations. We calculated L at the fixpoints assuming a dipole magnetic field. L then becomes a function of the height h, the Earth radius R_e, and the magnetic latitude λ

$$L = \frac{\left(1 + \frac{h}{R_e}\right)}{\cos^2(\lambda)} \tag{7}$$

One of the student teams at the 2023 COSPAR-IRI Workshop in South Korea compared the L-values determined with this simple method versus the more realistic values found with the multipole IGRF model. They found that above 3000 km the agreement is within 5% in the −60° to +60° magnetic latitude range. Another point to consider is the fact that the 30,000 km fixpoint will generally be outside the plasmasphere and its electron density should be at least an order of magnitude lower than the plasmaspheric model prediction. A point that could be easily introduced when incorporating the extension option into IRI. The same might be true for the 20,000 km fixpoint especially during storm-induced plasmasphere suppression. However, this upper part of the plasmasphere will not have a significant impact on the combined ionosphere-plasmasphere *TEC*, which is the primary parameter for which this plasmaspheric extension is introduced into IRI.

4. Conclusions

The International Reference Ionosphere (IRI) is the international standard for the representation of parameters in Earth's ionosphere and is widely used for applications in many different areas of applied and theoretical sciences, engineering and education as shown in Fig. 2. It is an example of successful international collaboration involving 66 experts representing 27 countries worldwide (Fig. 1). The wide usage of the model is illustrated by the many

journals covering a wide range of subjects that have published articles that cited the IRI model (Fig. 2). With the help of data assimilation and adjusted indices it is possible to bring the climatological IRI model closer to real-time conditions and many studies have been published on this topic (Tables 1 and 2).

The special focus of this paper is the representation of the electron density in the topside and in the plasmasphere, because they play such an important role in determining the total electron content (TEC) a parameter of special interest for many IRI users.

The topside electron density profile is normalized to *NmF2* and *hmF2* and the latest version IRI-2020 provides 4 options for the topside electron density profile. Three of these options, IRI2001, IRI2001cor and IRICOR2 are related to the very first topside model that was developed by Rawer et al. (1978a, b,c) and Rawer (1984). IRI2001 model was successfully improved with correction terms determined by Bilitza (2004) and Bilitza and Xiong (2021) leading to the topside options IRI2001cor and COR2, respectively. A comprehensive evaluation of all four options by Pignalberi et al. (2024) with GRACE, ICON, and DMSP in-situ data has pointed to remaining issues that need to be resolved for the two best performing options COR2 and NeQuick. The COR2 option, while describing the low latitude topside with associated EIA phenomenology remarkably well, still shows a solar activity trend in the upper topside. The NeQuick option represents the lower and upper topside quite well, but still needs to counter-balance the propagation of the EIA features to higher altitude.

Empirical modelling of the electron density distribution in the topside and in the plasmasphere has been to a large part proceeding separately. However, there is no clear boundary between ionosphere and plasmasphere. The most often used demarcation is the transition from the O^+ dominated ionosphere to H^+ and He^+ domination higher up. But other definitions have been proposed as well (Lee et al., 2016). For IRI the exact separation point between the two spheres is not important. A seamless transition from topside to plasmasphere domain is the IRI goal. Currently, a user can achieve this goal by extrapolating the IRI topside formalism into the plasmasphere and this can be done with either one of the topside options as well as the IRI-Plas version. But this approach for the plasmaspheric part is not data-based as the rest of the IRI model and as requested by the IRI-sponsoring organizations COSPAR and URSI. Topside sounder data may have been used for supporting the extrapolation, but only up to 3,000 km. For the rest of the plasmasphere the general assumption in this approach is a smooth continuation of the topside density decay for the vertical profile throughout the plasmasphere. But the plasmaspheric electron density is best modelled through its L-shell dependence and not its vertical height dependence. And as the IMAGE RPI data showed (Ozhogin et al., 2012) variation along the magnetic field line also need to be considered.

In this paper we propose a different approach. There have been numerous empirical models developed for the plasmasphere as discussed in section 3.1. We propose to apply the Booker (1977) method to connect an empirical plasmasphere model to the IRI topside profile. This approach gives equal weight to both regions and does not require a special merging function or normalization to an ionospheric foot point. We have evaluated three plasmasphere models that have been often used and cited (Carpenter and Anderson, 1992; Gallagher et al., 2000; Ozhogin et al., 2012). An important criterion was also that they were developed with data acquired during different satellite missions with different measurement techniques. For the evaluation of these models, we selected three data sets that were acquired by three different satellite missions with different measurement techniques (DE-1/RIMS, IMAGE/RPI, CRRES/PWE). We find that the Ozhogin et al. (2012) and Carpenter and Anderson (1992) models perform equally well and better than the Gallagher et al. (2000) model. Our recommendation is to use the Ozhogin et al. (2012) model as the IRI default, because it performed well and is the only model that considers density variations along the magnetic field line. As a second option we recommend the inclusion of the Gallagher et al. (2000) model since its performance was quite different from the other two. This will encourage users to compare these two models with other data sources and support the continued evaluation of the two models. Our study is a first step towards fully including a plasmaspheric extension in IRI. Our plasmaspheric extension model does not yet include a plasmapause and is not reliable in the polar cap region. For the polar cap region, the model developed by Nsumei et al. (2008) with IMAGE/RPI data is a good candidate and we intend to investigate this and other models for the polar cap and plasmapause region in a follow-on study.

Data availability statement. The DE-1/RIMS and IMGAGE/RPI data used in this study are available from NASA's Space Physics Data Facility (SPDF) at https://spdf.gsfc.nasa.gov/pub/data/. The CRRES/PWE data are available at https://doi.org/10.7302/250x-bt08. The IRI software and information about the model can be obtained from the IRI homepage at https://irimodel.org/.

Acknowledgements. This article is a contribution to the celebration of the 25th Anniversary of the Founding of the Istituto Nazionale di Geofisica e Vulcanologia. We thankfully acknowledge the invitation to be part of this celebration.

References

Aa, E., S. Liu, W. Huang, L. Shi et al. (2016). Regional 3-D Ionospheric electron density specification on the basis of data assimilation of ground-based GNSS and radio occultation data, Adv Space Res., 14, 6, 433-448, doi:10.1002/2016SW001363.

An, X., X. Meng, W. Jiang, H. Chen et al. (2019). Global ionosphere estimation based on data fusion from multisource: Multi-GNSS, IRI model, and satellite altimetry, J. Geophys. Res. Space Phys., 124, 7, 6012-6028, doi:10.1029/2019JA026896.

Anderson, R. R., D. A. Gurnett and D. L. Odem (1992). CRRES Plasma Wave Experiment, J. Spacecraft Rockets, 29, 4, 570-573, doi:10.2514/3.25501.

Angling, M. J., J. Shaw, A. K. Shukla and P. S. Cannon (2009). Development of an HF selection tool based on the Electron Density Assimilative Model near-real-time ionosphere, Radio Sci., 44, RS0A13, doi:10.1029/2008RS004022.

Benson, R. F. and D. Bilitza (2009). New satellite mission with old data: Rescuing a unique data set, Radio Sci., 44, RS0A04, doi:10.1029/2008RS004036

Bent, R. B., S. K. Llewellyn and P. E. Schmid (1972). Description and evaluation of the Bent ionospheric model, Volume 1-3, Space and Missile Systems Organization, Report SAMSO TR-72-081, National Technical Information Service, Springfield, Virginia (NTIS).

Bilitza, D. (1986). International Reference Ionosphere: Recent Developments, Radio Sci. 21, 343-346, doi:10.1029/RS021i003p00343.

Bilitza, D. (1990). International Reference Ionosphere 1990, National Space Science Data Center (NSSDC), 155, Greenbelt, Maryland, USA, NSSDC/WDC-A-R&S 90-22.

Bilitza, D. (1997). International Reference ionosphere – Status 1995/96, Adv. Space Res., 20, 9, 1751-1754, doi:10.1016/S0273-1177(97)00584-X.

Bilitza, D. (2001). International Reference Ionosphere 2000, Radio Sci., 36, 2, 261-275, doi:10.1029/2000RS002432

Bilitza, D. (2004). A correction for the IRI topside electron density model based on Alouette/ISIS topside sounder data, Adv. Space Res., 33, 6, 838-843, doi:10.1016/j.asr.2003.07.009.

Bilitza, D. (2009). Evaluation of the IRI-2007 model options for the topside electron density, Adv. Space Res., 44, 6, 701-706, doi:10.1016/j.asr.2009.04.036.

Bilitza, D., K. Rawer and S. Pallaschke (1988). Study of ionospheric models for satellite orbit determination, Radio Sci., 23, 3, 223-232, doi:10.1029/RS023i003p00223.

Bilitza, D., S. Bhardwaj and C. Koblinsky (1997). Improved IRI predictions for the GEOSAT time period, Adv. Space Res., 20, 9, 1755-1760, doi:10.1016/S0273-1177(97)00585-1.

Bilitza, D., X. Huang, B. Reinisch, R. Benson et al. (2004). Topside Ionogram Scaler With True Height Algorithm (TOPIST): Automated processing of ISIS topside ionograms, Radio Sci., 39, 1, RS1S27, doi:10.1029/2002RS002840

Bilitza, D. and B. W. Reinisch (2008). International Reference Ionosphere 2007: Improvements and new parameters, Adv. Space Res., 42, 4, 599-609, doi:10.1016/j.asr.2007.07.048.

Bilitza, D., L.-A. McKinnell, B. Reinisch and T. Fuller-Rowell (2011). The International Reference Ionosphere (IRI) today and in the future, J. Geod., 85, 12, 909-920, doi:10.1007/s00190-010-0427-x.

Bilitza, D., S. A. Brown, M. Y. Wang, J. R. Souza et al. (2012). Measurements and IRI Model Predictions during the Recent Solar Minimum, J. Atmos. Solar-Terrestrial Phys., 86, 99-106, doi:10.1016/j.jastp.2012.06.010.

Bilitza, D., D. Altadill, Y. Zhang, C. Mertens et al. (2014). The International Reference Ionosphere 2012 – a model of international collaboration, J. Space Weather Space Clim., 4, A07, 1-12, doi:10.1051/swsc/2014004.

Bilitza, D., D. Altadill, V. Truhlik, V. Shubin et al. (2017). International Reference Ionosphere 2016: From ionospheric climate to real-time weather predictions, Adv Space Res., 15, 418-429, doi:10.1002/2016SW001593.

Bilitza, D. and C. Xiong (2021). A solar activity correction term for the IRI topside electron density model, Adv. Space Res., 68, 5, 2124-2137, doi:10.1016/j.asr.2020.11.012.

Bilitza, D., M. Pezzopane, V. Truhlik, D. Altadill et al. (2022). The International Reference Ionosphere model: A review and description of an ionospheric benchmark, Rev. Geophys., 60, e2022RG000792, doi:10.1029/2022RG000792.

Booker, H. G. (1977). Fitting of multi-region ionospheric profiles of electron-density by a single analytic-function of height, J. Atmos. Terr. Phys., 39, 5, 619-623, doi:10.1016/0021-9169(77)90072-1.

Brown, S., D. Bilitza and E. Yiğit (2018). Ionosonde-Based Indices for Improved Representation of Solar Cycle Variation in the International Reference Ionosphere Model, J. Atmos. Terr. Phys., 171, 137-146, doi:10.1016/j.jastp.2017.08.022.

Carpenter, D. L. and R. R. Anderson (1992). An ISEE/Whistler model of equatorial electron density in the magnetosphere, J. Geophys. Res., 97, A2, 1097-1108, doi:10.1029/91JA01548.

Chou, M.-Y., J. Yue, J. Wang, J. D. Huba et al. (2023). Validation of Ionospheric Modeled TEC in the Equatorial Ionosphere During the 2013 March and 2021 November Geomagnetic Storms, Adv Space Res, 21, 6, e2023SW003480, doi:10.1029/2023SW003480.

Coïsson, P., S. M. Radicella, R. Leitinger and B. Nava (2006). Topside electron density in IRI and NeQuick: Features and limitations, Adv. Space Res., 37, 5, 937-942, doi:10.1016/j.asr.2005.09.015.

Denton, R. E., K. Takahashi, I. A. Galkin, P. A. Nsumei et al. (2006). Distribution of density along magnetospheric field lines, J. Atmos. Terr. Phys., 111, A4, A04213, doi:10.1029/2005JA011414.

Fridman, S. V., L. J. Nickisch, M. Aiello and M. Hausman (2006). Real-time reconstruction of the three-dimensional ionosphere using data from a network of GPS receivers, Radio Sci., 41, 5, RS5S12, doi:10.1029/2005RS003341.

Galkin, I. A., B. W. Reinisch, X. Huang and D. Bilitza (2012). Assimilation of GIRO data into a real-time IRI, Radio Sci., 47, 4, RS0L07, doi:10.1029/2011RS004952.

Galkin, I. A., B. W. Reinisch, A. M. Vesnin, D. Bilitza et al. (2020). Assimilation of sparse continuous Near-Earth Weather Measurements by NECTAR Model Morphing, Adv Space Res., 18, e2020SW002463, doi:10.1029/2020SW002463.

Gallagher, D. L., P. D. Craven and R. H. Comfort (2000). Global core plasma model, J. Geophys. Res., 105, A8, 18819-18833, doi:10.1029/1999JA000241.

Gulyaeva, T. L. (2003). Variations in the half width of the topside ionosphere according to the observations by space ionosondes ISIS 1, ISIS 2, and IK 19, Int. J. Geomagn. Aeron., 4, 3, 201-207, URL: https://api.semanticscholar.org/CorpusID:198184499.

Gulyaeva, T. L. and J. E. Titheridge (2006). Advanced specification of electron density and temperature in the IRI ionosphere-plasmasphere model, Adv. Space Res., 38, 11, 2587-2595, doi:10.1016/j.asr.2005.08.045

Guo, D., S. Fu, Z. Xiang, B. Ni et al. (2021). Prediction of dynamic plasmapause location using a neural network, Adv Space Res., 19, e2020SW002622, doi:10.1029/2020SW002622.

Habarulema, J. B. and N. Ssessanga (2016). Adapting a climatology model to improve estimation of ionosphere parameters and subsequent validation with radio occultation and ionosonde data, Adv Space Res, 15, 1, 84-98, doi:10.1002/2016SW001549.

Hartley, D. P., G. S. Cunningham, J.-F. Ripoll, D. M. Malaspina et al. (2023). Using Van Allen Probes and Arase observations to develop an empirical plasma density model in the inner zone. J. Atmos. Terr. Phys., 128, 3, e2022JA031012, doi:10.1029/2022JA031012.

Hernández-Pajares, M., J. M. Juan, J. Sanz and D. Bilitza (2002), Combining GPS measurements and IRI model values for Space Weather specification, Adv. Space Res., 29, 6, 949-958, doi:10.1016/S0273-1177(02)00051-0.

Hu, T., X. Xu and J. Luo (2024). Multi-source data ingestion for IRI-2020 model: a combination of ground-based and space-borne observations, GPS Solution 28, 78 (2024), doi:10.1007/s10291-024-01620-y.

Jakowski, N. and M. M. Hoque (2018). A new electron density model of the plasmasphere for operational applications and services, J. Space Weather Space Clim., 8, A16, 15, doi:10.1051/swsc/2018002.

Jeong S.-H., Y. H. Kim, J.-H. Kim and Y.-S. Kwak (2022). A regional ionospheric assimilation study with GPS and COSMIC measurements using a 3D-var algorithm (IDA4D), Adv. Space Res., 69, 6, 2489-2500, doi:10.1016/j.asr.2021.12.049.

Ji, E.-Y., Y.-J. Moon and E. Park (2020). Improvement of IRI global TEC maps by deep learning based on conditional Generative Adversarial Networks, Adv Space Res, 18, 5, e2019SW002411, doi:10.1029/2019SW002411.

Kashcheyev, A. and B. Nava (2019). Validation of NeQuick 2 model topside ionosphere and plasmasphere electron content using COSMIC POD TEC, J. Geophys. Res. Space Phys.124, 11, 9525-9536, doi:10.1029/2019JA026971.

Klenzing, J., F. Simões, S. Ivanov, D. Bilitza et al. (2013). Performance of the IRI-2007 model for equatorial topside ion density in the African sector for low and extremely low solar activity, Adv. Space Res., 52, 10, 1780-1790, doi:10.1016/j.asr.2012.09.030.

Klenzing, J., F. Simões, S. Ivanov, R. A. Heelis et al. (2011). Topside equatorial ionospheric density and composition during and after extreme solar minimum, J. Geophys. Res.116, A12, A12330, doi:10.1029/2011JA017213.

Kimura, I., A. Hikuma, Y. Kasahara and H. Oya (1996). Electron density distribution in the plasmasphere in conjunction with IRI model, deduced from Akebono wave data, Adv. Space Res., 18, 6, 279-288, doi:10.1016/0273-1177(95)00937-X.

Komjathy, A., R. Langley and D. Bilitza (1998). Ingesting GPS-Derived TEC Data into the International Reference Ionosphere for single Frequency Radar Altimeter Ionospheric Delay Corrections, Adv. Space Res., 22, 6, 793-801, doi:10.1016/S0273-1177(98)00100-8.

Lee, H.-B., Y. H. Kim, E. Kim, J. Hong et al. (2016). Where does the plasmasphere begin? Revisit to topside ionospheric profiles in comparison with plasmaspheric TEC from Jason-1, J. Geophys. Res. Space Phys., 121, 10,091-10,102, doi:10.1002/2016JA022747.

Li, Q., L. Liu, J. Jiang, W. Li, H. Huang, Y. Yu et al. (2019). α-Chapman scale height: Longitudinal Variation and Global Modeling. J. Geophys. Res. Space Phys., 124, 3, 2083-2098, doi:10.1029/2018JA026286.

Lin, C. Y., T. Matsuo, J. Y. Liu, C. H. Lin et al. (2017). Data assimilation of groundbased GPS and radio occultation total electron content for global ionospheric specification, J. Geophys. Res. Space Phys., 122, 10,876-10,886, doi:10.1002/2017JA024185.

Liu, L., M. He, W. Wan, and M.-L. Zhang (2008). Topside ionospheric scale heights retrieved from Constellation Observing System for Meteorology, Ionosphere, and Climate radio occultation measurements, J. Geophys. Res. Space Phys., 113, A10304, doi:10.1029/2008JA013490.

Lühr, H. and C. Xiong (2010). The IRI 2007 model overestimates electron density during the 23/24 solar minimum, Geophys. Res. Lett. 37, 23, L23101, doi:10.1029/2010GL045430.

Mao, W., M. Peifeng and J. Tang (2024). Mapping high spatial resolution ionospheric total electron content by integrating Time Series InSAR with International Reference Ionosphere model, ISPRS J. Photogramm. Remote Sens., 214, 153-166, doi:10.1016/j.isprsjprs.2024.06.003.

Mengist, C. K., N. Ssessanga, S.-H. Jeong, J.-H. Kim et al. (2019). Assimilation of multiple data types to a regional ionosphere model with a 3D-Var algorithm (IDA4D), Sp. Weather., 17, 7, 1018-1039, doi:10.1029/2019SW002159.

Migoya-Orué, Y. O., S. M. Radicella and B. Nava (2013). Comparison of topside electron density computed by ionospheric models and plasma density observed by DMSP satellites., Adv. Space Res., 52, 10, 1710-1716, doi:10.1016/j.asr.2013.01.032.

Migoya-Orué, Y., B. Nava, S. Radicella and K. Alazo-Cuartas (2015). GNSS derived TEC data ingestion into IRI 2012, Adv. Space Res. 55, 8, 1994-2002, doi:10.1016/j.asr.2014.12.033.

Moldwin, M. B., L. Downward, H. K. Rassoul, R. Amin et al. (2002). A new model of the location of the plasmapause: CRRES results, J. Geophys. Res., 107, A11, SMP 2-1-SMP 2-9, doi:10.1029/2001JA009211.

Moldwin, M. B. (2024). NASA CRRES Plasma Wave Instrument Electron Density Data [Data set], Univ. Mich – Deep Blue Data, doi:10.7302/250x-bt08.

Mingjie, Lv., C. Zhou, T. Liu, J. Qiao et al. (2022). High-Frequency Channel Modeling Based on the Multi-Source Ionospheric Assimilation Model, Remote Sens., 14, 17, 4133, doi:10.3390/rs14174133

Nava, B., P. Coïsson and S. M. Radicella (2008). A new version of the NeQuick ionosphere electron density model, J. Atmos. Sol.-Terr. Phys., 70, 15, 1856-1862, doi:10.1016/j.jastp.2008.01.015.

Nsumei, P. A., B. W. Reinisch, P. Song, J. Tu et al. (2008). Polar cap electron density distribution from IMAGE radio plasma imager measurements: Empirical model with the effects of solar illumination and geomagnetic activity, J. Geophys. Res. Space Phys., 113, A01217, doi:10.1029/2007JA012566.

Ozhogin, P., J. Tu, P. Song and B. W. Reinisch (2012). Field-aligned distribution of the plasmaspheric electron density: An empirical model derived from the IMAGE RPI measurements, J. Geophys. Res. Space Phys., 117, A06225, doi:10.1029/2011JA017330.

Pezzopane, M. and A. Pignalberi (2019). The ESA Swarm mission to help ionospheric modeling: A new NeQuick topside formulation for mid-latitude regions. Sci. Rep., 9, 1, 12253, doi:10.1038/s41598-019-48440-6.

Pezzopane, M., M. Pietrella, A. Pignatelli, B. Zolesi et al. (2011). Assimilation of autoscaled data and regional and local ionospheric models as input sources for real-time 3-D International Reference Ionosphere modeling, Radio Science, 46, 5, RS5009, doi:10.1029/2011RS004697.

Pezzopane, M., A. Pignalberi and B. Nava (2023). On the low-latitude NeQuick topside ionosphere mismodelling: the role of parameters H0, g, and r, Adv. Space Res., 72, 4, 1224-1236, doi:10.1016/j.asr.2023.04.014.

Pezzopane, M., A. Pignalberi, M. Pietrella, H. Haralambous et al. (2024). An Update of the NeQuick-Corr Topside Ionosphere Modeling Based on New Datasets, Atmosphere, 15, 4: 498, doi:10.3390/atmos15040498.

Pierrard, V., E. Botek, J.-F. Ripoll, S. A. Thaller et al. (2021). Links of the plasmapause with other boundary layers of the magnetosphere: ionospheric convection, radiation belt boundaries, auroral oval, Front. Astron. Space Sci., 8, 728531, doi:10.3389/fspas.2021.728531

Pignalberi, A., M. Pezzopane, R. Rizzi and I. Galkin (2018). Effective solar indices for ionospheric modeling: a review and a proposal for a real-time regional IRI, Surv. Geophys., 39, 125-167, doi:10.1007/s10712-017-9438-y.

Pignalberi, A., M. Pezzopane, R. Rizzi and I. Galkin (2018b). Correction to: Effective Solar Indices for Ionospheric Modeling: A Review and a Proposal for a Real-Time Regional IRI. Surv. Geophys., 39(1), 169-169. doi:10.1007/s10712-017-9453-z.

Pignalberi, A., M. Pezzopane and B. Nava, (2022). Optimizing the NeQuick topside scale height parameters through COSMIC/FORMOSAT-3 Radio Occultation Data, IEEE Geosci. Remote Sens. Lett., 19, 1-5. doi:10.1109/LGRS.2021.3096657.

Pignalberi, A., C. Cesaroni, M. Pietrella, M. Pezzopane et al. (2024a). Ionospheric Nowcasting Over Italy Through Data Assimilation: A Synergy Between IRI UP and IONORING, Sp. Weather., 22, 5, e2023SW003838, doi:10.1029/2023SW003838.

Pignalberi, A., D. Bilitza, P. Coïsson, H. Haralambous et al. (2024b). Validation of the IRI2020 topside ionosphere options through in-situ electron density observations by low-Earth-orbit satellites, Adv. Space Res., ISSN: 0273-1177doi:10.1016/j.asr.2024.05.056.

Prol, F. S., M. Hernández-Pajares, P. O. Camargo and M. T. A. H. Muella, (2018). Spatial and temporal features of the topside ionospheric electron density by a new model based on GPS radio occultation data, J. Geophys. Res. Space Phys., 123, 3, 2104-2115, doi:10.1002/2017JA024936.

Prol, F. S., D. Themens, M. Hernández-Pajares, P. O. Camargo et al. (2019). Linear vary-chap topside electron density model with topside sounder and radio-occultation data, Surveys in Geophysics, 40, 277-293, doi:10.1007/s10712-019-09521-3.

Prol, F. S., A. G. Smirnov, M. M. Hoque and Y. Y. Shprits (2022). Combined model of topside ionosphere and plasmasphere derived from radio-occultation and Van Allen Probes data, Scientific Reports, 12, 9732, doi:10.1038/s41598-022-13302-1.

Radicella, S. M. and R. Leitinger (2001). The evolution of the DGR approach to model electron density profiles, Adv. Space Res., 27, 1, 35-40, doi:10.1016/S0273-1177(00)00138-1.

Rawer, K. (Ed.) (1974). Methods of Measurements and Results of Lower Ionosphere Structure, Akademie-Verlag, Berlin, G.D.R., 462.

Rawer, K. (1984). Modelling of neutral and ionized atmospheres, in Encyclopedia of Physics, XLIX/7, Springer-Verlag, Berlin, Germany, 223-533.

Rawer, K., D. Bilitza and S. Ramakrishnan (1978a). Goals and status of the International Reference Ionosphere, Rev. Geophys., 16, 2, 177-181, doi:10.1029/RG016i002p00177.

Rawer, K., D. Bilitza and S. Ramakrishnan (1978b). International Reference ionosphere 78, Special Report, International Union of Radio Science (URSI), Brussels, Belgium.

Rawer, K., D. Bilitza, S. Ramakrishnan and N. Sheikh (1978c). Intentions and build-up of the International reference Ionosphere, in Operational Modelling of the Aerospace Propagation Environment, AGARD Conference Proceedings No. 238, 6-1–6-9.

Reinisch, B. W., P. Nsumei, X. Huang and D. Bilitza (2007). Modeling the F2 Topside and Plasmasphere for IRI Using IMAGE/RPI and ISIS Data, Adv. Space Res., 39, 5, 731-738, doi:10.1016/j.asr.2006.05.032.

Reinisch, B. W., X. Huang, P. Song, J. L. Green et al. (2004). Plasmaspheric mass loss and refilling as a result of a magnetic storm, J. Geophys. Res. Space Phys., 109, A01202, doi:10.1029/2003JA009948.

Ripoll, J.-F., V. Pierrard, G. S. Cunningham, X. Chu et al. (2023). Modeling of the cold electron plasma density for radiation belt physics, Front. Astron. Space Sci., 10, 1096595, doi:10.3389/fspas.2023.1096595.

Rycroft, M. J. and I. R. Jones (1985). Modelling the plasmasphere for the international reference ionosphere, Adv. Space Res., 5, 10, 21-27, doi:10.1016/0273-1177(85)90175-9.

Rycroft, M. J. and I. R. Jones (1987). A suggested model for the IRI plasmapheric distribution, Adv. Space Res., 7, 6, 13-22, doi:10.1016/0273-1177(87)90266-3.

Schmidt, M., D. Bilitza, C. K. Shum and C. Zeilhofer (2008). Regional 4-D modeling of the ionospheric electron density, Adv. Space Res. 42, 4, 782-790, doi:10.1016/j.asr.2007.02.050.

Servan-Schreiber, N., M. Aggarwal, Y. Huang, M. Kang et al. (2024). Validation of the IRI-2020 model for the topside-plasmasphere using GNSS TEC measurements, Adv. Space Res., doi:10.1016/j.asr.2024.07.009.

Shim, J. S., M. Kuznetsova, L. Rastätter, M. Hesse et al. (2011). CEDAR Electrodynamics Thermosphere Ionosphere 1 (ETI) Challenge for Systematic Assessment of Ionosphere/Thermosphere Models: NmF2, hmF2, and Vertical Drift Using Ground-Based Observations, Sp. Weather., 9, 12, S12003, doi:10.1029/2011SW000727.

Shim, J. S., M. Kuznetsova, L. Rastätter, M. Hesse et al. (2012). CEDAR Electrodynamics Thermosphere Ionosphere (ETI) Challenge for systematic assessment of ionosphere/thermosphere models: Electron density, neutral density, NmF2, and hmF2 using space-based observations, Sp. Weather., 10, S10004, doi:10.1029/2012SW000851.

Shim, J. S., M. Kuznetsova, L. Rastätter, D. Bilitza et al. (2014). Systematic Evaluation of Ionosphere/Thermosphere (IT) Models, Modeling the Ionosphere-Thermosphere System" è Mod. Ionosphere-Thermosphere Syst., John Wiley & Sons, Ltd, Chichester, UK, doi:10.1002/9781118704417.ch13.

Shim, J. S., L. Rastätter, M. Kuznetsova, D. Bilitza et al. (2017). CEDAR-GEM challenge for systematic assessment of Ionosphere/thermosphere models in predicting TEC during the 2006 December storm event, Sp. Weather., 15, 1238-1256, doi:10.1002/2017SW001649.

Shim, J. S., I. Tsagouri, L. Goncharenko, L. Rastaetter et al. (2018). Validation of ionospheric specifications during geomagnetic storms: TEC and foF2 during the 2013 March storm event, Sp.Weather., 16, 1686-1701, doi:10.1029/2018SW002034.

Singh, A. K., H. Haralambous and C. Oikonomou (2021). Validation and improvement of NeQuick topside ionospheric formulation using COSMIC/FORMOSAT-3 data, J. Geophys. Res. Space Phys., 126, 4, e2020JA028720, doi:10.1029/2020JA028720.

Smirnov, A., Y. Shprits, F. Prol et al. (2023). A novel neural network model of Earth's topside ionosphere, Sci. Rep., 1303, doi:10.1038/s41598-023-28034-z.

Ssessanga, N., H. Y. Kim, E. Kim and J. Kim (2015). Regional optimization of IRI-2012 output (TEC, foF2) using derived GPS-TEC, JKPS, 66, 10, 1599-1610, doi:10.3938/jkps.66.1599.

Ssessanga, N., Y. H. Kim, J. B. Habarulema and Y.-S. Kwak (2019). On imaging South African Regional Ionosphere using 4D-var technique, Sp. Weather., 17, 11, 1584-1604, doi:10.1029/2019SW002321.

Stankov, S. M. and N. Jakowski (2006). Topside ionospheric scale height analysis and modelling based on radio occultation measurements, Journal of Atmospheric and Solar-Terrestrial Physics, 68, 2, 134-162, doi:10.1016/j.jastp.2005.10.003.

Strangeways, H. J. (1986). A model for the electron temperature variation along geomagnetic field lines and its effect on electron density profiles and VLF paths, J. Atmos. Terr. Phys., 48,7, 671-683, doi:10.1016/0021-9169(86)90016-4

Themens, D. R., P. T. Jayachandran, D. Bilitza, P. J. Erickson et al. (2018). Topside electron density representations for middle and high latitudes: A topside parameterization for E-CHAIM based on the NeQuick, J. Geophys. Res.: Space Phys., 123, 2, 1603-1617, doi:10.1002/2017JA024817.

Truhlik, V., D. Bilitza and L. Triskova (2012). A new global empirical model of the electron temperature with the inclusion of the solar activity variations for IRI, EPS., 64, 531-443, doi:10.5047/eps.2011.10.016.

Truhlik, V., D. Bilitza and L. Triskova (2015). Towards better description of solar activity variation in the International Reference Ionosphere topside ion composition model, Adv. Space Res., 55, 8, 2099-2105, doi:10.1016/j.asr.2014.07.033.

Truhlík, V., D. Bilitza, D. Kotov, M. Shulha et al. (2021). Global Empirical Model of the Ion Temperature in the Ionosphere for the International Reference Ionosphere, Atmosphere, 12, 8, 1081, doi:10.3390/atmos12081081.

Webb, P. A., Y. Wang, L. N. Garcia, R. F. Benson et al. (2010). Electron Density Dataset from IMAGE RPI Magnetospheric Dynamic Spectra, https://spdf.gsfc.nasa.gov/pub/data/image/rpi/rpi_Ne_fp_along_orbit/IMAGE_RPI_electron_density_dataset_description.pdf.

Wenjing, L., M. Limberger, M. Schmidt, D. Dettmering et al. (2015). Regional modeling of ionospheric peak parameters using GNSS data: an update for IRI, Adv. Space Res., 55, 8, 1981-1993, doi:10.1016/j.asr.2014.12.006.

Williams, D. V., M. J. Rycroft, A. J. Smith, V. V. Bezrukikh et al. (1981). Intercomparison of various measurements of thermal plasma densities at and near the plasmapause, Adv. Space Res., 1,1, 235-238, doi:10.1016/0273-1177(81)90114-9.

Yue, X., W. S. Schreiner, Y.-H. Kuo, D. C. Hunt et al. (2012). Global 3-D ionospheric electron density reanalysis based on multi-source data assimilation, J. Geophys. Res., Space Phys., 117, A09325, doi:10.1029/2012JA017968.

Zeilhofer, C., M. Schmidt, D. Bilitza and C. K. Shum (2009). Regional 4-D modeling of the ionospheric electron density from satellite data and IRI, Adv. Space Res., 43, 11, 1669-1675, doi:10.1016/j.asr.2008.09.033.

Zhang, Y-L., L. J. Paxton and D. Bilitza (2010). Near real-time assimilation of auroral peak E-region density and equatorward boundary in IRI, Adv. Space Res., 46, 8, 1055-1063, doi:10.1016/j.asr.2010.06.029.

Zhelavskaya, I. S., Shprits, Y. Y. and M. Spasojevic (2017). Empirical modeling of the plasmasphere dynamics using neural networks, J. Geophys. Res., Space Phys., 122, 11, 227-11, 244, doi:10.1002/2017JA024406.

***CORRESPONDING AUTHOR: Dieter BILITZA**,
George Mason University, Department of Physics and Astronomy, Fairfax, USA
e-mail: dbilitza@gmu.edu